TDMA Based Numerical Approach on Modeling of Charge Carrier Transport and Ion Vacancy Motion in Perovskite Solar Cells

Daniyal Khosh Maram
Department of Electrical Engineering,
Amirkabir University of Technology
Tehran, Iran
Danialkhoshmaram@aut.ac.ir

Abstract

Drift-diffusion models that account for the motion of both electronic and ionic charges are important tools for explaining the hysteretic behaviour. Furnishing numerical solutions to such models for realistic operating conditions is challenging owing to the extreme values of some of the parameters. We present a finite difference scheme with time step that provides second order accuracy in the mesh spacing. The method is able to use realistic parameters values whilst providing high accuracy. Also, three diagonal matrix approximation (TDMA) method is exploit due to matrix solve simplification. This method is robust and fast way to solve. Ion vacancy density, electron concentration, and hole concentration profiles are calculated in transient time-scale. In following, built-in potential is varied and profiles are illustrated. This approach paves the way to have a better insight of device physics and its related phenomena such as ionic motion, hysteresis.

Index Terms

Perovskite, device physics, ion vacancy migration, drift-diffusion, charge transport model, dimensionless model, three diagonal matrix approximation (TDMA).

I. Introduction

Recently improvement in power conversion efficiency (PCE) of perovskite solar cell (PSC) in which has increased enormously from around 3% to above 20% within five years and makes this type of solar cells a attractive topic [1]–[4]. Also outstanding optoelectronic properties made perovskite materials as absorber layers in thin-film architectures [5], [6]. The growth development of PSCs is a remarkably intense area of research because of high performance, facile processing methods, and low cost of manufacture [7]–[9]. The PSCs integrate based on the typical structure of PSCs consisting of the perovskite absorber that is sandwiched between a hole transport layer (HTL) and an electron transport layer (ETL). Generally, methylammonium lead tri-iodide ($CH_3NH_3PbI_3$) is using as a perovskite absorbing material in PSCs [10]. Spiro-MeOTAD is using as a common material for HTL and also titanium dioxide (TiO_2) for ETL. According to the conduction band of HTL and the valence band of ETL, the transport layer materials are chosen in which the conduction band in the HTL is above that in the perovskite, and the valence band in the ETL is below in the perovskite [11]. In the perovskite structure for leading holes towards the HTL and electrons towards the ETL, could be using of generating a built-in electric field arising from the discrepancies in the band energies of the different layers and these make a potential barrier exists to the entry of electrons into HTL and holes into ETL from perovskite [12]. Long-timescale transient behavior occurring on the order of tens of seconds is one of the distinguishing characteristics of PSCs. According to the current transients [13], [14] and according to current-voltage (J-V) curves, there is a phenomenon which has been termed hysteresis by the field [14], [15]. Various approaches can be used to the modeling of PSCs, including density functional theory (DFT), drift-diffusion models of charge carriers, and ion motion to equalizing the parameters of devices. DFT calculations are incapable of describing the behavior of a full cell, but practically they are used to obtain estimates of macroscopic quantities from the atomistic structures of the materials forming the device including ion vacancy densities and mobilities [16]. To describe the motion of electrons, holes, and ion vacancies drift-diffusion models are used in which these models are applicable on the nanometre length scale and upward, such as [17]–[21]. However, these works except [22], [23] use unrealistic parameter. Also, probably this because of ion accumulation/depletion at the edges of the perovskite layer in which cause extreme numerical stiffness of the problem owing to very narrow (~2 nm) Debye (boundary) layers. Eames et al. performed DFT calculations and obtained estimates for the equilibrium ion vacancy density and mobility [16] and based on this a combined numerical and asymptotic approach presented by Richardson et al. in which the electrical properties of the Debye layers modeled

by a non-linear surface capacitance [23]. That work was to demonstrate experimental J–V hysteresis data explained by the motion of ion vacancies in the perovskite layer. Since computational costs are some expensive causes that DFT can only be used to a few atoms and extremely short timescales, On the other hand, equivalent circuit models although are facile to solve, but they are arduous to connect directly to the device physics. A common pathway leading to a flexible computational model that can be directly interpreted in terms of device physics and is yielded by equivalently drift-diffusion or charge transport modeling. Prominently, this method permits to incorporated parameters in which obtained from DFT calculations of perovskite structure into the model [24]. At first, ion movements in PSCs was not recognized as a significant model and also as a result of charge transport models that treated the only hole and electron carrier was expressed. Afterward, models incorporating ion movements were examined. The newly developed methods for additional physics in this revised model have compelled. To date, numerical approaches are just using to obtain solutions for simplified models. The presented solution methods in [21], [25] are based on decoupling the relatively slow ion motion from the charge carrier transport. Decoupling the relatively slow ion movement from the charge carrier transport is base of the solution methods in Ref. [21], [25]. In Ref. [26] ion motion is decoupled from those carriers in which ion accumulation included in the form of narrow layers of uniform charge adjacent to each interface in the perovskite. Under illumination, accidental photons with energies above the bandgap are absorbed in the perovskite layer and generate an exciton that rapidly dissociates into a free electron which towards ETL and a hole which towards HTL [27]. Approximations have been utilized due to the incorporation of realistic densities of ion vacancies (as high as 10^{19} cm^{-3} [28]) resulting in a computationally challenging to determine model because of narrow Debye layers across which rapid changes in solution occur, the significant disparity between the timescales for ion vacancy motion and electron and hole transport, and substantial changes in the magnitude of the solution across the device [29]. In these studies, the analysis depends on approximation, including the assumption that the carrier densities remain extremely smaller than the ion vacancy density the pertinent experimental method whereas these approximations are convincing in most scenarios and lead to authentic approximate solutions, numerical treatment of the full system of equations that is capable of furnishing solutions across all relevant timescales, and operating regimes without simplification are highly desirable [29]. In this paper, aims to present a numerical scheme for obtaining authentic solutions to a fully coupled charge transport model of a PSC. The tridiagonal matrix algorithm (TDMA) has been used, which is a facilitated form of Gaussian elimination that can be applied to determine the tridiagonal system of equations. Although the TDMA is a direct method for 1D situation, it can be applied iteratively in a line-by-line method to solve multi-dimensional problems. The TDMA is an efficient way of solving tridiagonal matrix systems and utilized because it is fast, and tridiagonal matrices often occur in practice [30].

II. MATERIAL & METHOD

Here we formulated a charge transport model based on the typical structure of PSCs consisting of the perovskite absorber that is sandwiched between HTL and ETL. To treating these layers as quasi-metals, doped transport layers are utilized and cause the electric potential equal and uniform to that on their contacts. Also, this structure approximated to a single-layer model that all the relevant physics can be applied within the perovskite layer. The model describes the critical physical processes including motion, generation, and recombination of highly mobile charge carriers and their interaction with anion vacancies and a uniformly distributed stationary cation vacancy distribution. This work aims to solve this model using numerical method and details presented in [9], [25]. Notably, the numerical scheme that utilized for the single-layer model also can be extended to more realistic multi-layer models.

A. Physics Model in PSCs

In order, the model equations are presented in a dimensionless form to present the most straightforward possible method. The critical variables in the problem are time, t; the perpendicular distance from the interface of the perovskite layer with the ETL, x; the mobile anion vacancy density, P; the free-electron density, n; the hole density, p; the electric field (in the x-direction), E; the electric potential, the anion vacancy flux (in the x-direction), F_P; and the electron and hole current densities, J_n and j_p, respectively. The dimensionless model consists of three conservation equations for the three mobile charged species [29]:

$$\frac{\partial P}{\partial t} + \lambda \frac{\partial F^P}{\partial x} = 0 \tag{1}$$

$$\nu \frac{\partial n}{\partial t} = \frac{\partial j^n}{\partial x} + G(x) - R(n, p) \tag{2}$$

$$\nu \frac{\partial p}{\partial t} = -\frac{\partial j^p}{\partial x} + G(x) - R(n, p) \tag{3}$$

where F^P, j^n and j^p are [29]:

$$F^P = -\left(\frac{\partial P}{\partial x} + P\frac{\partial \phi}{\partial x}\right) \tag{4}$$

$$j^n = \kappa_n\left(\frac{\partial n}{\partial x} - n\frac{\partial \phi}{\partial x}\right) \tag{5}$$

$$j^p = -\kappa_p\left(\frac{\partial p}{\partial x} + p\frac{\partial \phi}{\partial x}\right) \tag{6}$$

in which G(x) and R(n, p) represent rates of charge carrier generation and recombination, respectively. These conservation equations couple to Poisson's equation [29]:

$$\frac{\partial E}{\partial x} = \frac{1}{\lambda^2}\left(P - 1 + \delta\left(p - n\right)\right) \tag{7}$$

where E is:

$$E = -\frac{\partial \phi}{\partial x} \tag{8}$$

B. Definition of dimensionless variables and parameters

The dimensional counterparts of the variables used in the model which we denote by a star, are retrieved from the following rescaling [29]:

$$\begin{aligned}
&x^* = bx, \quad t^* = \frac{L_d b}{D_+}t, \quad \Phi^* = V_T\Phi, \quad \Phi^*_{bi} = V_T\Phi_{bi},\\
&p^* = \frac{F_{ph}b}{\hat{D}}p, \quad n^* = \frac{F_{ph}b}{\hat{D}}n, \quad P^* = N_0 P, \quad j^{p*} = qF_{ph}j^p,\\
&j^{n*} = qF_{ph}j^n, \quad F^{p*} = \frac{D_+ N_0}{b}F^p, \quad G^* = \frac{F_{ph}}{b}G, \quad R^* = \frac{F_{ph}}{b}R,\\
&R^*_l = F_{ph}R_l, \quad R^*_r = F_{ph}R_r.
\end{aligned} \tag{9}$$

Here b denotes the width of the perovskite layer, L_d the Debye length, D_+ the anion vacancy diffusion coefficient, q the charge, V_T the thermal voltage , F_{ph} the incident photon flux, $\hat{D}$ a typical electronic charge carrier diffusivity and N_0 the equilibrium anion vacancy density. The Debye length is calculated based on the most populous charged species, which in this instance is the anion vacancies, as follows [29]:

$$L_d = \left(\frac{\varepsilon kT}{q^2 N_0}\right)^{1/2} \tag{10}$$

$$\begin{aligned}
&\nu = \frac{D_+ b}{\hat{D}L_d}, \quad \kappa_p = \frac{D_p}{\hat{D}}, \quad \kappa_n = \frac{D_n}{\hat{D}}, \quad \lambda = \frac{L_d}{b}\\
&\delta = \frac{F_{ph}b}{\hat{D}N_0}, \quad \bar{n} = \frac{n_b\hat{D}}{F_{ph}b}, \quad \bar{p} = \frac{p_b\hat{D}}{F_{ph}b}, \quad \Phi_{bi} = \frac{V_{bi}}{V_T}
\end{aligned} \tag{11}$$

where D_n and D_p are free-electron and hole diffusivities, respectively, and n_b and p_b are the dimensional electron density on the ETL interface and the dimensional hole density on the HTL interface, respectively. In [29] it is shown that, for a typical planar device formed by a methylammonium lead tri-iodide perovskite absorber layer sandwiched between a titania ETL layer and a spiro HTL layer, the dimensionless parameters take the values [11], [29]:

$$\begin{aligned}
&\nu = 1.4\times10^{-10}, \quad \kappa_p = 1, \quad \kappa_n = 1, \quad \lambda = 1\times10^{-2}\\
&\delta = 5.2\times10^{-8}, \quad \bar{n} = 82, \quad \bar{p} = 1.2, \quad \Phi_{bi} \approx 40.
\end{aligned} \tag{12}$$

C. Numerical Simplification Scheme

The method of lines is the basis of our numerical scheme. The spatial derivatives are discretized using second-order accurate finite differences. The discrete system is forming as a system of coupled differential-algebraic equations (DAEs) because the governing equation of the electric potential is elliptic. As such, temporal integration requires a specialized algorithm. Also, accuracy satisfying with respect to time-scaling transient are to be considered. The basis equations are provided below. By placing and solving the equations we get the following [29]:

$$\frac{\partial P}{\partial t} + \lambda \frac{\partial}{\partial x}\left(-\frac{\partial P}{\partial x} + PE\right) = 0 \tag{13}$$

$$\nu \frac{\partial n}{\partial t} = \frac{\partial j^n}{\partial x} + G(x) - R(n,p) \tag{14}$$

$$\nu \frac{\partial p}{\partial t} = -\frac{\partial j^p}{\partial x} + G(x) - R(n,p) \tag{15}$$

D. Discretization of Equations

Finite difference method is a discrete approximation computation approach for differential equations; its calculation results are not a continuous function in the domain but the approximate value of the functions at each mesh point. The basic idea of the difference method is to use different coefficients to replace the derivative part in the equations. In this simulation, it assumes the thickness of perovskite is L nm, and discretises the domain [0, L] with the distance of h. Here, in order to obtain convenient calculation and accurate results, nested grid method is used to discretise the device. Based on the discretisation model of the device, the Poisson's equation and continuity equations with the discrete form can be described below. For the electrons and holes a Dirichlet-type boundary condition is to be imposed on x = 0 and x = 1, whilst a specified value of the flux is to be imposed at the boundary x = 1 and x = 0, respectively [29]. Here ion vacancy density, P, related equation is discretized, as shown below [29]:

$$\begin{aligned} &\frac{P_i^{t+1} - P_i^t}{\Delta t} - \lambda \frac{P_{i+1} - 2P_i + P_{i-1}}{\Delta x^2} \\ &\quad + \lambda\left(-\frac{\phi_{i+1} - \phi_i}{\Delta x}\right)\left(\frac{P_{i+1} - P_i}{\Delta x}\right) \\ &\quad + \lambda P_i\left(-\frac{\phi_{i-1} - 2\phi_i + \phi_{i+1}}{\Delta x^2}\right) = 0 \end{aligned} \tag{16}$$

Here the boundary conditions are provided [29]:

$$\begin{aligned} &\begin{cases} i = 1 \\ x = 0 \end{cases} \rightarrow \frac{\partial P}{\partial x} - PE = 0 \rightarrow \frac{P_i - P_{i-1}}{\Delta x} + P_i\left(\frac{\partial \phi}{\partial x}\right) = 0 \\ &\qquad \rightarrow P_{i-1} = P_i\left(1 + \Delta x\left(\frac{\partial \phi}{\partial x}\right)\right) \\ &\begin{cases} i = N \\ x = 1 \end{cases} \rightarrow \frac{\partial P}{\partial x} - PE = 0 \rightarrow \frac{P_{i+1} - P_i}{\Delta x} + P_i\left(\frac{\partial \phi}{\partial x}\right) = 0 \\ &\qquad \rightarrow P_{i+1} = P_i\left(1 + \Delta x\left(-\frac{\partial \phi}{\partial x}\right)\right) \end{aligned} \tag{17}$$

Then, electron density, n, related equation is provided below [29]:

$$\begin{aligned} \nu \frac{n_i^{t+1} - n_i^t}{\Delta t} &= \kappa_n\left(\frac{n_{i+1}^{t+1} - 2n_i^{t+1} + n_{i-1}^{t+1}}{\Delta x^2}\right) - \kappa_n n_i^{t+1}\left(\frac{\phi_{i+1} - 2\phi_i + \phi_{i-1}}{\Delta x^2}\right) \\ &\quad - \kappa_n\left(\frac{\phi_{i+1} - \phi_i}{\Delta x}\right)\left(\frac{n_{i+1}^{t+1} - n_i^{t+1}}{\Delta x}\right) + G(x) - R(n,p) \end{aligned} \tag{18}$$

Here the boundary conditions are provided [29]:

$$\begin{cases} i = 1 \\ x = 0 \end{cases} \rightarrow n_i = \bar{n}$$
$$\begin{cases} i = N \\ x = 1 \end{cases} \rightarrow \left(\frac{\partial n}{\partial x} + nE\right) = -\frac{R_r(n)}{\kappa_n} \rightarrow \frac{n_{i+1} - n_i}{\Delta x} - n_i \frac{\partial \phi}{\partial x} = -\frac{R_r(n)}{\kappa_n} \tag{19}$$
$$\rightarrow n_{i+1} = -\frac{R_r(n)}{\kappa_n}\Delta x + n_i \Delta x \frac{\partial \phi}{\partial x} + n_i$$

Then, hole density, p, related equation is assumed and simplified [29]:

$$\nu \frac{p_i^{t+1} - p_i^t}{\Delta t} = \kappa_p \left(\frac{p_{i+1}^{t+1} - 2p_i^{t+1} + p_{i-1}^{t+1}}{\Delta x^2}\right) + \kappa_p p \left(\frac{\partial^2 \phi}{\partial x^2}\right) + \kappa_p \left(\frac{\partial \phi}{\partial x}\right)\left(\frac{p_{i+1} - p_i}{\Delta x}\right) + G - R \tag{20}$$

Here the boundary conditions are provided [29]:

$$\begin{cases} i = 1 \\ x = 0 \end{cases} \rightarrow \left(\frac{\partial p}{\partial x} + pE\right) = -\frac{R_l(p)}{\kappa_p} \rightarrow \frac{p_{i+1} - p_i}{\Delta x} - p_i \frac{\partial \phi}{\partial x} = -\frac{R_l(p)}{\kappa_p}$$
$$\rightarrow p_{i+1} = -\frac{R_l(p)}{\kappa_p}\Delta x - p_i \Delta x \frac{\partial \phi}{\partial x} + p_i \tag{21}$$
$$\begin{cases} i = N \\ x = 1 \end{cases} \rightarrow p_i = \bar{p}$$

Also, Poisson's equation becomes:

$$-\left(\frac{\phi_{i+1} - 2\phi_i + \phi_{i-1}}{\Delta x^2}\right) = \frac{1}{\lambda^2}\left(P_i - 1 + \delta\left(p - n\right)\right) \tag{22}$$

III. Result

We verify the performance of the scheme utilizing physically relevant test cases. Here we are comparing our numerical results to the asymptotic solution presented in [5] in the particular case where the bulk recombination, R(n, p), is monomolecular (depending solely on the local hole concentration p) and the surface recombination rates, are both zero, such that [29]:

$$R(n, p) = \gamma\left(\frac{np - N_i^2}{n + \varepsilon p + K_3}\right) \tag{23}$$

$$R(n, p) = \gamma p, \quad R_r(n) = R_l(p) = 0. \tag{24}$$

Here γ is a dimensionless rate constant. As noted in [9], when hole pseudo-lifetime is much higher than electron pseudo-lifetime, monomolecular hole-dominated bulk recombination is the limit of the Shockley-Read-Hall (SRH) recombination law. Also describes recombination in the perovskite material methylammonium lead tri-iodide [31]. The numerical scheme that presented hither is easily capable of dealing with nonlinear recombination rates such as the full SRH law. Generally, in such applications, we presume that the photo-generation rate, G(x), obeys the Beer-Lambert law, which has the dimensionless form [29].

$$G(x) = \Upsilon \exp(-\Upsilon x) \tag{25}$$

in which Υ is the dimensionless absorption length. Estimates of these from [11], [29] are:

$$\Upsilon = 0.92, \quad \gamma = 0.15 \tag{26}$$

A simple choice of initial conditions satisfying the boundary conditions is [29]:

$$P_{init} = 1, \quad n_{init} = \bar{n}, \quad p_{init} = \bar{p}. \tag{27}$$

Practically, choosing of primary conditions is not crucial for the modeling of PSCs because it is standard practice to include a pre-conditioning step in any experimental procedure [29].

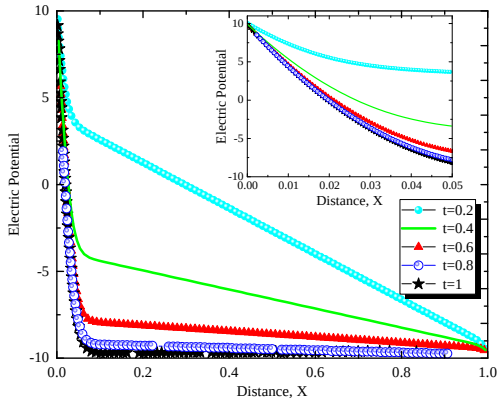

Fig. 1: Electric potential profile in time-scale t=0.2, 0.4, 0.6, 0.8, 1, at phi=20v.

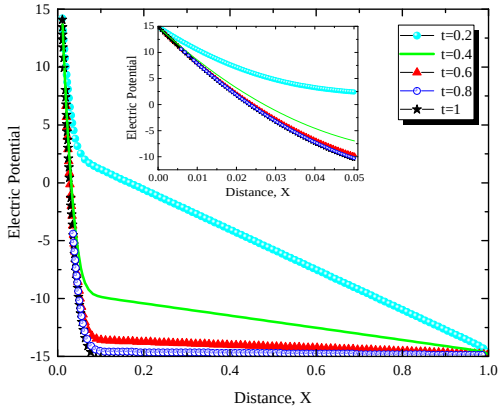

Fig. 2: Electric potential profile in time-scale t=0.2, 0.4, 0.6, 0.8, 1, at phi=30v.

Reliable model with realistic parameters, with experimental results, which were reported in [29] is compared with our proposed numerical method with simplified TDMA approach. There is an agreement between our calculated results with those reported in Ref. [29]. In following, to prove flexibility of our proposed numerical method, possible reported parameters are instantiated and utilized to investigate ion vacancy P, electron density n, and hole density p profiles for a cell with perovskite width 150 nm thinner perovskite layer which a cell with 600 nm perovskite layer width has reported in [11], [29]. Real device estimated parameters were illustrated in [11]. Based on this data, the dimensionless parameters are assumed. In following, it is desirable to investigate ion vacancy density P, electron density n, and hole density p profiles with respect to transient time-scaling. It facilitates better insight of device physics matters such as ionic motion in perovskite, hysteresis, stability criterion and correlated phenomena. ETL and HTL are considered as quasi-metals, as highly doped layers. Therefore, single-layer model approximation which is capable of relevant physics justification, can be applied within the perovskite layer. After that, we consider a device with different Φ_{bi} to observe this parameters role in profiles. It is noteworthy to mentioned that $V_{bi} = \Phi_{bi} \times V_T$, V_{bi} as a built-in voltage, determined by the difference in the Fermi levels in the TiO_2 and the spiro layers, gives rise to an electric field $\frac{V_{bi}}{b}$ in the perovskite layer. This field drives positive charges towards the spiro layer and negative charges towards the TiO_2. At short circuit, free electron-hole pairs are separated by this field to create a current in which electrons are extracted through the TiO_2 layer and holes are extracted through the spiro layer. A positive applied bias, V, produces an electric field that opposes the built-in field.In the absence of charge build up within the perovskite there is a net electric field $\frac{(V_{bi}-V)}{b}$ from left to right. When $V < V_{bi}$, this field drives the positively charged iodide vacancies into the region of the perovskite adjacent to its interface with the spiro. Here we demonstrate profiles changes with built-in potential variation respect to transient time-scale for Φ_{bi}=20, 30, and 40. Electric potential, electron concentration, hole concentration, and ion vacancy density profiles are provided in Fig.(1) - Fig.(12).

IV. Conclusion

This paper mainly introduces a numerical model for perovskite solar cell and a specific computation and algorithm process for Poisson's and continuity equations. The simulation results are obtained by using the MATLAB program.

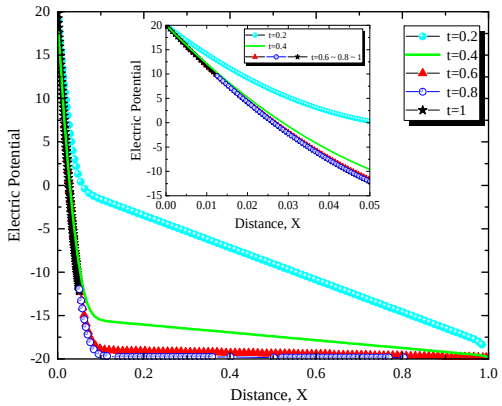

Fig. 3: Electric potential profile in time-scale t=0.2, 0.4, 0.6, 0.8, 1, at phi=40v.

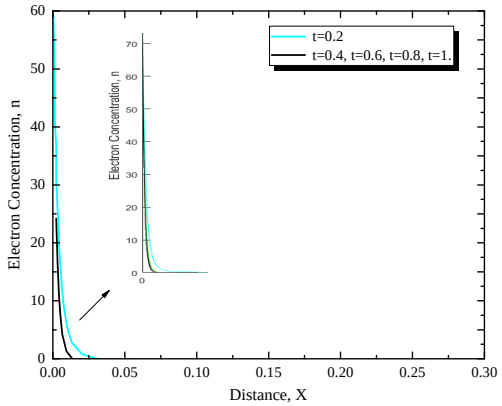

Fig. 4: Electron concentration profile in time-scale t=0.2, 0.4, 0.6, 0.8, 1, at phi=20v.

We have utilized a numerical scheme for determining PDE drift-diffusion model of ion vacancy and charge carrier transport in a PSC. This numerical scheme to reduce the system of PDEs to a system of ordinary differential-algebraic equations utilizes second-order finite difference approximations of spatial derivatives. The proposed numerical scheme utilized for the single-layer model. Therefore, these approaches can be extended to more realistic multi-layer models in upcoming researches.

V. Conflict of Interest

There is no conflict of interest.

References

[1] G. Niu, X. Guo, and L. Wang, "Review of recent progress in chemical stability of perovskite solar cells," J. Mater. Chem. A, vol. 3, pp. 8970–8980, 2015.
[2] J.-P. Correa-Baena, A. Abate, M. Saliba, W. Tress, T. J. Jacobsson, M. Grätzel, and A. Hagfeldt, "The rapid evolution of highly efficient perovskite solar cells," Energy & Environmental Science, vol. 10, no. 3, pp. 710–727, 2017.
[3] G. Niu, X. Guo, and L. Wang, "Review of recent progress in chemical stability of perovskite solar cells," Journal of Materials Chemistry A, vol. 3, no. 17, pp. 8970–8980, 2015.
[4] D. K. Maram, H. Habibiyan, H. Ghafoorifard, and O. Shekoofa, "Analysis of optimum copper oxide hole transporting layer for perovskite solar cells," in 2019 27th Iranian Conference on Electrical Engineering (ICEE), pp. 214–219, April 2019.
[5] S. D. Stranks, G. E. Eperon, G. Grancini, C. Menelaou, M. J. Alcocer, T. Leijtens, L. M. Herz, A. Petrozza, and H. J. Snaith, "Electron-hole diffusion lengths exceeding 1 micrometer in an organometal trihalide perovskite absorber," Science, vol. 342, no. 6156, pp. 341–344, 2013.
[6] M. A. Green, Y. Jiang, A. M. Soufiani, and A. Ho-Baillie, "Optical properties of photovoltaic organic–inorganic lead halide perovskites," The journal of physical chemistry letters, vol. 6, no. 23, pp. 4774–4785, 2015.
[7] A. Mei, X. Li, L. Liu, Z. Ku, T. Liu, Y. Rong, M. Xu, M. Hu, J. Chen, Y. Yang, et al., "A hole-conductor–free, fully printable mesoscopic perovskite solar cell with high stability," Science, vol. 345, no. 6194, pp. 295–298, 2014.
[8] F. Fu, T. Feurer, T. Jäger, E. Avancini, B. Bissig, S. Yoon, S. Buecheler, and A. N. Tiwari, "Low-temperature-processed efficient semi-transparent planar perovskite solar cells for bifacial and tandem applications," Nature communications, vol. 6, p. 8932, 2015.

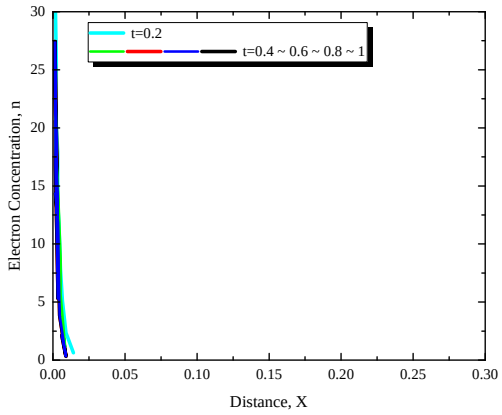

Fig. 5: Electron concentration profile in time-scale t=0.2, 0.4, 0.6, 0.8, 1, at phi=30v.

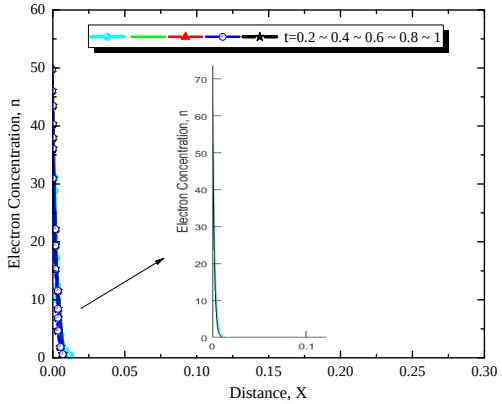

Fig. 6: Electron concentration profile in time-scale t=0.2, 0.4, 0.6, 0.8, 1, at phi=40v.

[9] N.-G. Park, "Organometal perovskite light absorbers toward a 20% efficiency low-cost solid-state mesoscopic solar cell," The Journal of Physical Chemistry Letters, vol. 4, no. 15, pp. 2423–2429, 2013.

[10] T. J. Jacobsson, J.-P. Correa-Baena, M. Pazoki, M. Saliba, K. Schenk, M. Grätzel, and A. Hagfeldt, "Exploration of the compositional space for mixed lead halogen perovskites for high efficiency solar cells," Energy & Environmental Science, vol. 9, no. 5, pp. 1706–1724, 2016.

[11] N. Courtier, J. M. Foster, S. O'KANE, A. Walker, and G. Richardson, "Systematic derivation of a surface polarisation model for planar perovskite solar cells," European Journal of Applied Mathematics, vol. 30, no. 3, pp. 427–457, 2019.

[12] P. Cui, D. Wei, J. Ji, H. Huang, E. Jia, S. Dou, T. Wang, W. Wang, and M. Li, "Planar p–n homojunction perovskite solar cells with efficiency exceeding 21.3%," Nature Energy, vol. 4, no. 2, p. 150, 2019.

[13] S. E. O'Kane, G. Richardson, A. Pockett, R. G. Niemann, J. M. Cave, N. Sakai, G. E. Eperon, H. J. Snaith, J. M. Foster, P. J. Cameron, et al., "Measurement and modelling of dark current decay transients in perovskite solar cells," Journal of Materials Chemistry C, vol. 5, no. 2, pp. 452–462, 2017.

[14] E. L. Unger, E. T. Hoke, C. D. Bailie, W. H. Nguyen, A. R. Bowring, T. Heumüller, M. G. Christoforo, and M. D. McGehee, "Hysteresis and transient behavior in current–voltage measurements of hybrid-perovskite absorber solar cells," Energy & Environmental Science, vol. 7, no. 11, pp. 3690–3698, 2014.

[15] H. J. Snaith, A. Abate, J. M. Ball, G. E. Eperon, T. Leijtens, N. K. Noel, S. D. Stranks, J. T.-W. Wang, K. Wojciechowski, and W. Zhang, "Anomalous hysteresis in perovskite solar cells," J. Phys. Chem. Lett, vol. 5, no. 9, pp. 1511–1515, 2014.

[16] C. Eames, J. M. Frost, P. R. Barnes, B. C. O'regan, A. Walsh, and M. S. Islam, "Ionic transport in hybrid lead iodide perovskite solar cells," Nature communications, vol. 6, p. 7497, 2015.

[17] P. Calado, A. M. Telford, D. Bryant, X. Li, J. Nelson, B. C. O'Regan, and P. R. Barnes, "Evidence for ion migration in hybrid perovskite solar cells with minimal hysteresis," Nature communications, vol. 7, p. 13831, 2016.

[18] K. Domanski, B. Roose, T. Matsui, M. Saliba, S.-H. Turren-Cruz, J.-P. Correa-Baena, C. Carmona, G. Richardson, J. Foster, F. Angelis, J. Ball, A. Petrozza, N. Mine, M. Nazeeruddin, W. Tress, M. Gräztel, U. Steiner, A. Hagfeldt, and A. Abate, "Migration of cations induces reversible performance losses over day/night cycling in perovskite solar cells," Energy & Environmental Science, vol. 2017, pp. 604–613, 2 2017.

[19] R. Gottesman, P. Lopez-Varo, L. Gouda, J. A. Jimenez-Tejada, J. Hu, S. Tirosh, A. Zaban, and J. Bisquert, "Dynamic phenomena at perovskite/electron-selective contact interface as interpreted from photovoltage decays," Chem, vol. 1, no. 5, pp. 776–789, 2016.

[20] H. Shen, D. A. Jacobs, Y. Wu, T. Duong, J. Peng, X. Wen, X. Fu, S. K. Karuturi, T. P. White, K. Weber, et al., "Inverted hysteresis in ch3nh3pbi3 solar cells: role of stoichiometry and band alignment," The journal of physical chemistry letters, vol. 8, no. 12, pp. 2672–2680, 2017.

[21] S. van Reenen, M. Kemerink, and H. J. Snaith, "Modeling anomalous hysteresis in perovskite solar cells," The journal of physical chemistry letters, vol. 6, no. 19, pp. 3808–3814, 2015.

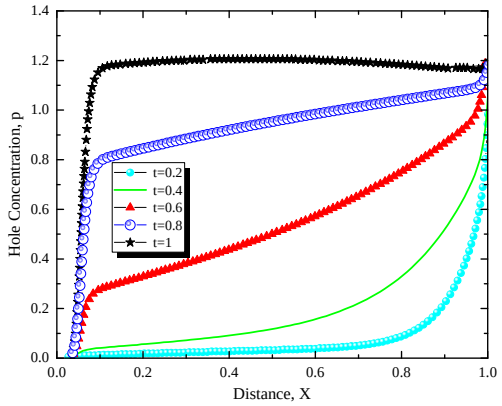

Fig. 7: Hole concentration profile in time-scale t=0.2, 0.4, 0.6, 0.8, 1, at phi=20v.

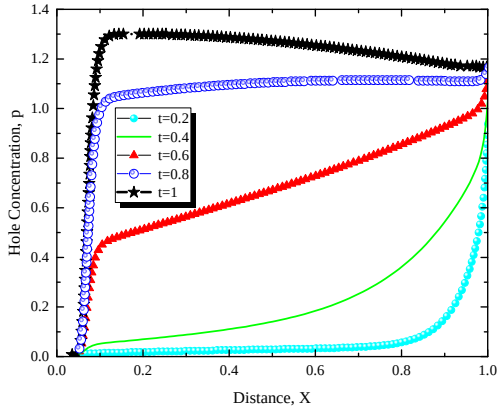

Fig. 8: Hole concentration profile in time-scale t=0.2, 0.4, 0.6, 0.8, 1, at phi=30v.

[22] S. E. O'Kane, G. Richardson, A. Pockett, R. G. Niemann, J. M. Cave, N. Sakai, G. E. Eperon, H. J. Snaith, J. M. Foster, P. J. Cameron, et al., "Measurement and modelling of dark current decay transients in perovskite solar cells," Journal of Materials Chemistry C, vol. 5, no. 2, pp. 452–462, 2017.

[23] G. Richardson, S. E. O'Kane, R. G. Niemann, T. A. Peltola, J. M. Foster, P. J. Cameron, and A. B. Walker, "Can slow-moving ions explain hysteresis in the current–voltage curves of perovskite solar cells?," Energy & Environmental Science, vol. 9, no. 4, pp. 1476–1485, 2016.

[24] G. Richardson, S. E. O'Kane, R. G. Niemann, T. A. Peltola, J. M. Foster, P. J. Cameron, and A. B. Walker, "Can slow-moving ions explain hysteresis in the current–voltage curves of perovskite solar cells?," Energy & Environmental Science, vol. 9, no. 4, pp. 1476–1485, 2016.

[25] R. Gottesman, P. Lopez-Varo, L. Gouda, J. A. Jimenez-Tejada, J. Hu, S. Tirosh, A. Zaban, and J. Bisquert, "Dynamic phenomena at perovskite/electron-selective contact interface as interpreted from photovoltage decays," Chem, vol. 1, no. 5, pp. 776–789, 2016.

[26] D. A. Jacobs, Y. Wu, H. Shen, C. Barugkin, F. J. Beck, T. P. White, K. Weber, and K. R. Catchpole, "Hysteresis phenomena in perovskite solar cells: the many and varied effects of ionic accumulation," Physical Chemistry Chemical Physics, vol. 19, no. 4, pp. 3094–3103, 2017.

[27] I. Koutselas, L. Ducasse, and G. C. Papavassiliou, "Electronic properties of three-and low-dimensional semiconducting materials with pb halide and sn halide units," Journal of Physics: Condensed Matter, vol. 8, no. 9, p. 1217, 1996.

[28] A. Walsh, D. O. Scanlon, S. Chen, X. Gong, and S.-H. Wei, "Self-regulation mechanism for charged point defects in hybrid halide perovskites," Angewandte Chemie International Edition, vol. 54, no. 6, pp. 1791–1794, 2015.

[29] N. E. Courtier, G. Richardson, and J. M. Foster, "A fast and robust numerical scheme for solving models of charge carrier transport and ion vacancy motion in perovskite solar cells," Applied Mathematical Modelling, vol. 63, pp. 329–348, 2018.

[30] P. V. Patil, "Finite volume numerical grid technique for multidimensional problems," 2014.

[31] S. George, J. M. Foster, and G. Richardson, "Modelling in vivo action potential propagation along a giant axon," Journal of mathematical biology, vol. 70, no. 1-2, pp. 237–263, 2015.

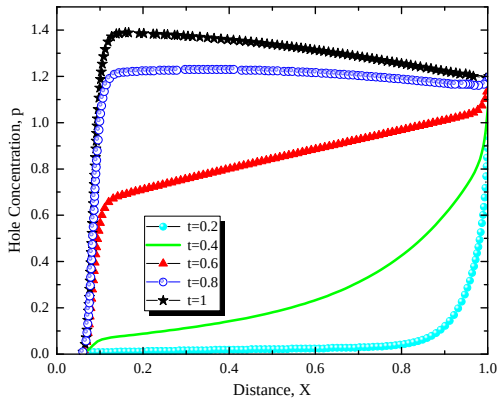

Fig. 9: Hole concentration profile in time-scale t=0.2, 0.4, 0.6, 0.8, 1, at phi=40v.

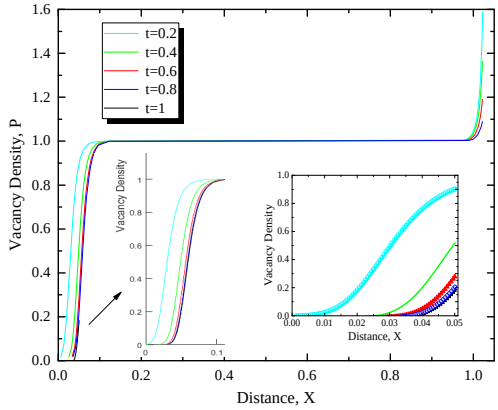

Fig. 10: Ion vacancy density profile in time-scale t=0.2, 0.4, 0.6, 0.8, 1, at phi=20v.

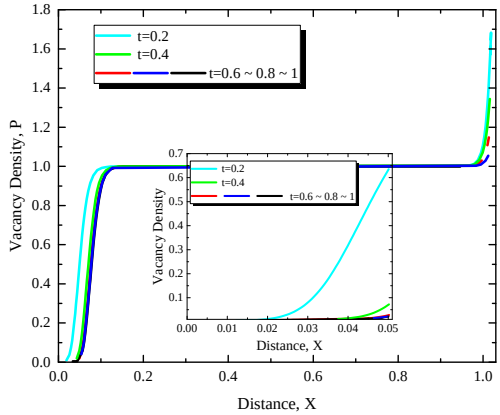

Fig. 11: Ion vacancy density profile in time-scale t=0.2, 0.4, 0.6, 0.8, 1, at phi=30v.

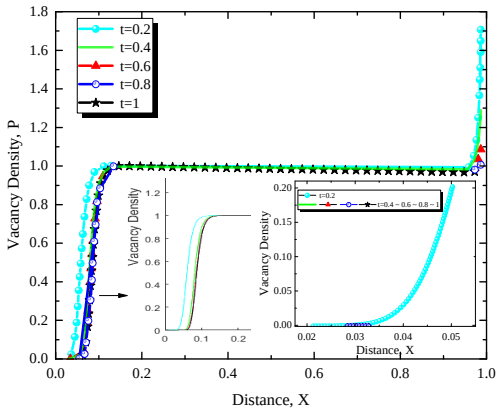

Fig. 12: Ion vacancy density profile in time-scale t=0.2, 0.4, 0.6, 0.8, 1, at phi=40v.